Structure of the Complex of Human Programmed Death 1, PD-1, and Its Ligand PD-L1

Zak, Krzysztof M.; Kitel, Radoslaw; Przetocka, Sara; Golik, Przemyslaw; Guzik, Katarzyna; Musielak, Bogdan; Dömling, Alexander; Dubin, Grzegorz; Holak, Tad A.

Published in:
Structure

DOI:
10.1016/j.str.2015.09.010

Publication date:
2015

Short Article

Structure

Structure of the Complex of Human Programmed Death 1, PD-1, and Its Ligand PD-L1

Graphical Abstract

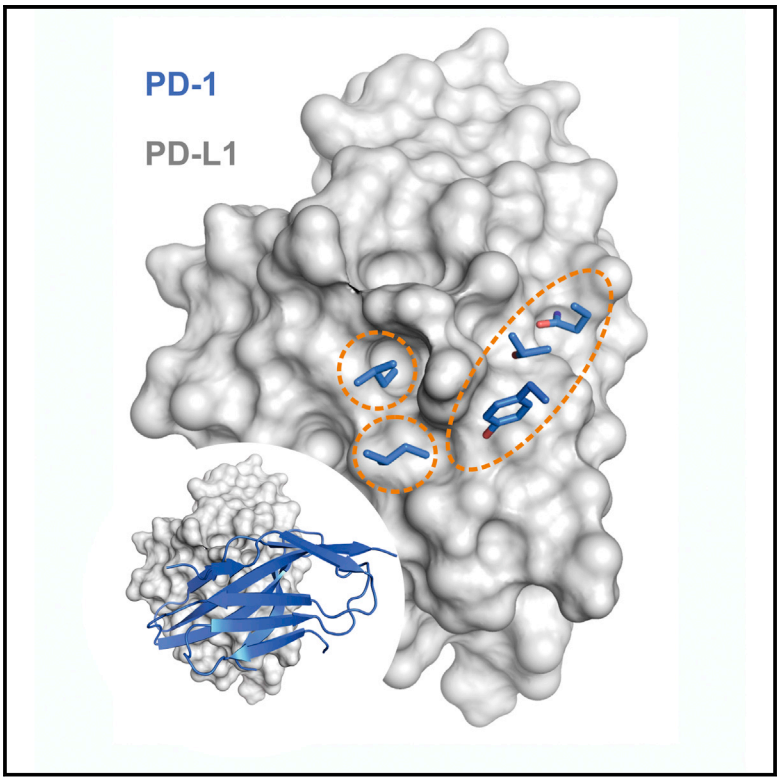

Authors

Krzysztof M. Zak, Radoslaw Kitel, Sara Przetocka, ..., Alexander Dömling, Grzegorz Dubin, Tad A. Holak

Correspondence

holak@chemia.uj.edu.pl (T.A.H.), grzegorz.dubin@uj.edu.pl (G.D.)

In Brief

Zak et al. reveal the molecular details of the human PD-1/PD-L1 interaction based on an X-ray structure of the complex. The authors elucidate that the ligand binding to human PD-1 is associated with significant plasticity within the receptor, and provide a detailed molecular map of the interaction surface.

Highlights

- Solved X-ray crystal structure of human PD-1/PD-L1 complex
- Identification of the main hot spots on PD-1 and PD-L1 surfaces
- Solved X-ray crystal structure of PD-1 binding domain from human PD-L1

Accession Numbers

4ZQK
5C3T

Zak et al., 2015, Structure *23*, 2341–2348
December 1, 2015
http://dx.doi.org/10.1016/j.str.2015.09.010

Structure
Short Article

Structure of the Complex of Human Programmed Death 1, PD-1, and Its Ligand PD-L1

Krzysztof M. Zak,[1,2] Radoslaw Kitel,[2,3] Sara Przetocka,[1,2] Przemyslaw Golik,[1,2] Katarzyna Guzik,[3] Bogdan Musielak,[3] Alexander Dömling,[4] Grzegorz Dubin,[1,2,*] and Tad A. Holak[2,3,5,*]
[1]Faculty of Biochemistry, Biophysics and Biotechnology, Jagiellonian University, Gronostajowa 7, 30-387 Krakow, Poland
[2]Malopolska Centre of Biotechnology, Jagiellonian University, Gronostajowa 7a, 30-387 Krakow, Poland
[3]Department of Organic Chemistry, Jagiellonian University, Ingardena 3, 30-060 Krakow, Poland
[4]Department for Drug Design, University of Groningen, A. Deusinglaan 9, 9713 AV Groningen, the Netherlands
[5]Max Planck Institute for Biochemistry, Am Klopferspitz 18, 82152 Martinsried, Germany
*Correspondence: holak@chemia.uj.edu.pl (T.A.H.), grzegorz.dubin@uj.edu.pl (G.D.)
http://dx.doi.org/10.1016/j.str.2015.09.010

SUMMARY

Targeting the PD-1/PD-L1 immunologic checkpoint with monoclonal antibodies has recently provided breakthrough progress in the treatment of melanoma, non-small cell lung cancer, and other types of cancer. Small-molecule drugs interfering with this pathway are highly awaited, but their development is hindered by insufficient structural information. This study reveals the molecular details of the human PD-1/PD-L1 interaction based on an X-ray structure of the complex. First, it is shown that the ligand binding to human PD-1 is associated with significant plasticity within the receptor. Second, a detailed molecular map of the interaction surface is provided, allowing definition of the regions within both interacting partners that may likely be targeted by small molecules.

INTRODUCTION

The immune system has an important role in controlling cancer. Tumor cells express cancer-specific antigens derived from genetic alterations, and as such are targeted by the immune cells. This response, however, is often inefficient, since tumors can actively suppress immunity (Tumeh et al., 2014). One of the mechanisms of that suppression involves interference with immunologic checkpoints (inhibitory receptors) on immune cells like, for example, the programmed death receptor 1 (PD-1), whereby cancer cells present negative immunologic regulators inducing exhaustion (loss of function) of antigen-specific effector T cells (Phan et al., 2015; Herbst et al., 2014; Topalian et al., 2015). A recent major breakthrough in cancer immunotherapy has emerged in immunologic checkpoint blockade, utilizing antibodies masking the inhibitory receptor PD-1 on immune effector cells or PD-1 inhibitory receptor ligand (PD-L1) on tumor cells, thereby alleviating cancer-induced immunosuppression (Herbst et al., 2014; Schumacher et al., 2015). This represents a major paradigm shift whereby the therapy aims at disinhibition of native immune response compared with previous approaches whereby tumor vaccines and recombinant cytokines aimed at its de novo activation. Another receptor from the family of immune-checkpoint receptors is the cytotoxic T-lymphocyte-associated antigen 4 (CTLA-4). Ipilimumab, a CTLA-4-blocking monoclonal antibody (mAb), became the first immune-checkpoint receptor targeted therapy accepted by the US Food and Drug Administration (FDA) in 2011 (Lipson and Drake, 2011; Dömling and Holak, 2014). Unfortunately, ipilimumab therapy is associated with frequent immune-mediated adverse events. Recent clinical trials with mAbs targeting the PD-1/PD-L1 pathway demonstrated impressive tumor responses, cleaner than mAbs against CTLA-4 (Lipson and Drake, 2011; Dömling and Holak, 2014; Powles et al., 2014; Topalian et al., 2015; Chen and Mellman, 2013; http://www.fda.gov/NewsEvents/Newsroom/PressAnnouncements/ucm436534.htm).

PD-1 is a type I transmembrane receptor that modulates the activity of T cells in peripheral tissues. An activated T cell expresses PD-1 on its surface upon antigen recognition and produces interferons which induce expression of PD-L1 in multiple tissues. Binding of PD-1 to its ligand limits T-cell activity. Thereby, under normal conditions, the PD-1/PD-L1 pathway prevents excessive stimulation and maintains the immune tolerance to self-antigens by negatively regulating the immune response (Riella et al., 2012). However, PD-L1 is often overexpressed in different tumors including lymphoma, melanoma, lung, breast cancer, glioblastoma, ovarian, kidney tumors, and bladder cancers, which results in immune response handicap within the tumor microenvironment (Sun et al., 2014; Muenst et al., 2013; Ahmadzadeh et al., 2009; Matsuzaki et al., 2010; Inman, 2007; Hawkes et al., 2015). The PD-1/PD-L1 interaction inhibits T-lymphocyte proliferation, release of cytokines, and cytotoxicity, resulting in exhaustion and apoptosis of tumor-specific T cells (Wherry, 2011). Blockage of the PD-1/PD-L1 interaction results in reversal of exhausted T-cell phenotype and normalization of antitumor response, providing the rationale of targeted therapy (Sakuishi et al., 2010). It is expected that similar reversal of exhausted T-cell phenotype may also provide a therapeutic advantage in chronic viral infections (Barber et al., 2006).

In clinics, a significant number of patients with melanoma demonstrated long-term responses to anti-PD1 immunotherapy (Hamid et al., 2013). The results were impressive enough to merit accelerated approval of nivolumab and

Table 1. Data Collection and Refinement Statistics

	Human PD-1/PD-L1 Complex	Apo-PD-1 Binding Domain from hPD-L1
Data Collection		
Space group	P 3_1 2 1	C 2 2 2_1
Cell dimensions		
a, *b*, *c* (Å)	70.86, 70.86, 114.36	53.00, 54.71, 84.90
α, β, γ (°)	90, 90, 120	90, 90, 90
Resolution (Å)	61.37–2.45 (2.53–2.45)[a]	42.45–1.8 (1.86–1.8)[a]
R_{merge}	0.043 (0.480)[a]	0.065 (0.391)[a]
$I/\sigma I$	35.22 (5.21)[a]	20.7 (4.9)[a]
Completeness (%)	99.98 (99.92)[a]	100 (100)[a]
Redundancy	10.6 (11.2)[a]	6.5 (6.7)[a]
Refinement		
Resolution (Å)	2.45	1.80
No. of reflections	12,708	11,799
R_{work}/R_{free}	0.2071/0.2527	0.1525/0.1777
No. of atoms		
Protein	1,650	1,035
Ligand/ion	1	-
Water	15	75
Average *B* factors		
Protein	57.60	17.50
Ligand/ion	50.10	-
Water	59.50	26.70
RMSDs		
Bond lengths (Å)	0.016	0.023
Bond angles (°)	1.77	2.23

[a]Values in parentheses represent the highest-resolution shell.

pembrolizumab (both target PD-1 blocking its interaction with PD-L1) by regulatory bodies in 2014 (Topalian et al., 2015; Dömling and Holak, 2014; http://www.fda.gov/NewsEvents/Newsroom/PressAnnouncements/ucm436534.htm). Recent evidence has even shown that anti-PD-1 therapy is superior to chemotherapy in the treatment of metastatic melanoma (Moreno and Ribas, 2015; Mahoney et al., 2015; Chen and Mellman, 2013). Nivolumab has also demonstrated unprecedented results in a clinical trial in metastatic squamous non-small cell lung cancer (NSCLC). It has recently gained FDA acceptance in this indication, becoming the first monotherapy in more than 15 years to demonstrate proven superior overall survival compared with the standard of care (http://www.fda.gov/Drugs/InformationOnDrugs/ApprovedDrugs/ucm436566.htm). Anti-PD-L1 immunotherapy is at the earlier stage of clinical development; nevertheless, several tested antibodies have also demonstrated highly encouraging results. Objective tumor responses were observed in early-phase clinical trials in melanoma, NSCLC, and several other solid tumors (Brahmer et al., 2012). Results obtained in a phase I clinical trial of patients with metastatic urothelial bladder cancer were so impressive (tumor shrinking was observed in 43% of patients) that the FDA granted a breakthrough designation for the tested antibody (Powles et al., 2014). It is currently widely expected that therapies directed against negative immunologic regulators (checkpoints) are likely to soon become a significant component of treatment for a variety of malignancies.

The excitement within the field encourages the development of small-molecule inhibitors of the PD-1/PD-L1 interaction that could likely overcome the typical drawbacks of the antibody-based immunotherapies, including certain side effects. This, however, is hindered, among other factors, by the incomplete structural information about these proteins. The structures of the complexes of the murine PD-1 and human PD-L1 (Lin et al., 2008) and that of the murine PD-1 and murine PD-L2 (Lázár-Molnár et al., 2008; Freeman, 2008), published in 2008, established the structural foundations of the PD-1/PD-L1, -2 interactions. These structures have not allowed, however, for assessment of the extent of plasticity in these interactions when starting from the apoprotein components of the complexes. The crystal structure of the extracellular domain of human PD-1 alone has only been determined recently PDB: 3RRQ. Despite the fact that the murine PD-1 binds human PD-L1, the sequence identity between human and murine PD-1 is only 64%, indicating likely differences in the details of the binding modes (Figure S1). Herein, we report the crystal structure of the human PD-1/human PD-L1 complex, which indeed documents significant differences in the binding between murine and human PD-1 and the ligand (hPD-L1). We also present a comprehensive comparison of the structures of the PD-1/PD-L1 complexes from different species and their components alone. This information allowed us to define features of the hot-spot pockets in human PD-1/PD-L1 required for inhibition of this interaction. The proposed pharmacophore model for this protein-protein interaction should provide a solid starting point for the design of chemical probes and potential small-molecule therapeutics targeting the PD-1/PD-L1 axis.

RESULTS

Overall Structure of the Human PD1/PD-L1 Complex

Crystals of the hPD-1/hPD-L1 complex that we obtained diffracted to 2.45 Å resolution and contained a single complex assembly in the asymmetric unit (Table 1). PD-1 assumes a β-sandwich immunoglobulin-variable (Ig V)-type topology with Cys54 and Cys123 forming a characteristic disulfide bridge; however PD-1 lacks the second disulfide common to other family members (CD28, CTLA-4, and ICOS). The molecule is well defined by electron density, safe for a region between C′D strands (Asp85–Asp92) (canonical Ig-strand designations are used; Figure S2). There is no indication of the PD-1 dimerization within the crystal lattice, consistent with its monomeric form in solution in previous reports (Lázár-Molnár et al., 2008; Zhang et al., 2004; Cheng et al., 2013).

Similarly to PD-1, the interacting, N-terminal domain of PD-L1 is also characterized by the Ig V-type topology. The entire molecule is well defined by its electron density. The arrangement of the molecules within the crystal lattice does not suggest dimerization of PD-L1 as has been presented in previous studies.

PD-1 and PD-L1 form a 1:1 complex within the crystal, consistent with the stoichiometry determined by us and others in solution (Lin et al., 2008; Cheng et al., 2013). This resolves the ambiguity concerning complex stoichiometry brought by

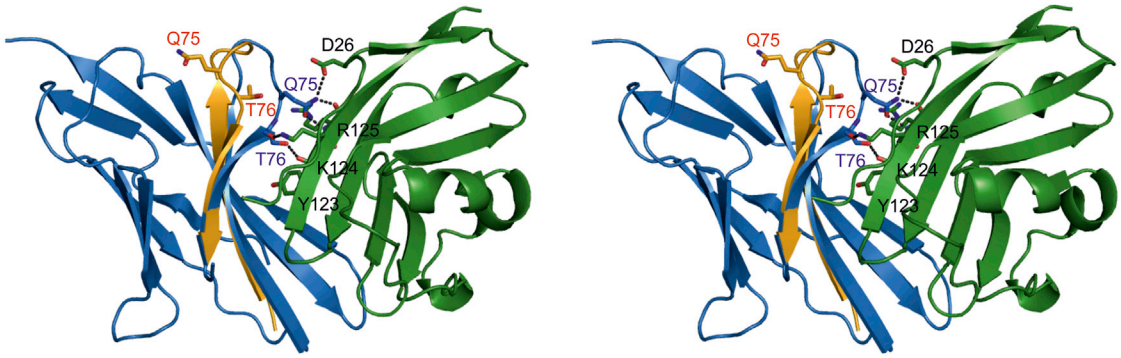

Figure 1. Binding of hPD-L1 Induces Significant Structural Rearrangements within the Structure of hPD-1

Within the complex structure, hPD-1 is colored blue and hPD-L1 is colored green; both are shown in stereo view in ribbon representation. Apo-hPD1 (PDB: 3RRQ) was overlaid on hPD-1 within the complex, and residues 62–82 of the former are shown (yellow ribbon). The structural rearrangement within the CC′ loop upon complex formation is clearly discernible.

the mPD-1/hPD-L1 structure where 2:1 stoichiometry was observed, although the interaction of one of the mPD-1 molecules was arbitrarily considered by the authors a crystallization artifact due to limited interaction surface (Lin et al., 2008). The 1:1 stoichiometry contrasts that observed within CTLA-4 complexes with its ligands, where both interacting partners form homodimers (Stamper et al., 2001; Schwartz et al., 2001). The interaction of PD-1 and PD-L1 resembles that of Ig V domains within antibodies and T-cell receptors being mediated by the strands from the front faces of interacting domains (GFCC′ β sheets). This places the two interacting partners roughly orthogonally such that the Ig V loops (CDR loops) do not take part in the interaction (as opposed to CTLA-4 interaction with its ligands where CDR loops provide the interaction surface), but rather form a structure resembling that of an antigen-binding site within antibodies. Consistently, the CDR3 (FG) loop important in the interaction of CTLA-4 with its ligands is not involved in PD-1/PD-L1 binding (Lin et al., 2008).

Ligand Binding Induces Conformational Changes within hPD-1

The crystal structure of apo-hPD-L1 in a monomeric form was determined here for reference, and is almost identical to that in the dimeric state PDB: 4Z18. The overall structure of apo-hPD-1 PDB: 3RRQ and the structures of apo-hPD-L1 determined by us and others (Zhang et al., 2004; Lin et al., 2008; Chen et al., 2010; and PDB: 4Z18) resemble those observed within the complex in this study. A more detailed analysis, however, demonstrates that complex formation involves significant structural flexibility, especially within hPD-1. The structure of apo-hPD-1 and the structure of hPD-1 extracted from the complex described within this study overlay relatively well (root-mean-square deviation [RMSD] of 0.388 Å) except for the CC′ loop (Met70-Asp77) (Figure 1). The loop is found in an open conformation in the apo-PD-1 structure where Met70 and Ser71 form a part of a C β strand within an antiparallel CF β sheet, and all the side chains within the loop point away from the ligand binding site. Complex formation induces loop rearrangement in a form of a 90° twist and associated ~5 Å displacement of C_α carbons. This results in even more pronounced displacements of the side-chain atoms. The $N_{\varepsilon 2}$ atom of Gln75 in free hPD-1 structure is located ~18 Å away from where the backbone atoms of $_L$Arg125 (the $_L$ symbol within amino acid designation refers to PD-L1) are located in the overlaid structure of the complex, whereas the side chain of Gln75 participates in hydrogen bonds with the backbone oxygen and amide of $_L$Arg125 within the complex. This rearrangement additionally allows hydrogen bond formation between the side chains of Gln75 and $_L$Asp26. In turn, the side-chain hydroxyl oxygen of Thr76 is translated by ~6 Å to facilitate hydrogen bond formation with the backbone carbonyl oxygen of $_L$Tyr123. A similar shift is observed for the backbone carbonyl oxygen of Thr76, which enables hydrogen bond formation with the side-chain amine of $_L$Lys124. The C and F β-sheet contacts mediated by Met70 and Ser71 in the apo-hPD-1 structure are lost during the CC′ loop rearrangement. Overall, the CC′ loop, found in an open conformation in apo-hPD-1, closes around hPD-L1, allowing formation of four hydrogen bonds. We hypothesize that this loop closure stabilizes the initial transient interaction of hPD-1 and hPD-L1. Interestingly, however, in the structure of apo-mPD-1 the CC′ loop displays a closed conformation, similar to that observed within the hPD-1/hPD-L1 and mPD-1/hPD-L1 complexes. Therefore, the described CC′ loop rearrangement is specific to human PD-1 only.

In contrast to hPD-1, the complex formation-associated plasticity within hPD-L1 involves only minor adjustments in the arrangement of the side chains contributing to the interaction surface and no significant changes within the backbone. The most pronounced movements involve the side chains of $_L$Glu58, $_L$Met115, $_L$Tyr123 (which form a hydrophobic pocket accommodating Ile134), $_L$Ile54, and $_L$Ala121. The majority of observed displacements, however, does not exceed 3 Å for the most distal side-chain atoms and, as such, may all be considered as minor adjustments imposed by local steric constraints of the interaction surface. Only the side chain of $_L$Arg113 displays a ~5 Å movement of the distal atoms. This allows formation of an intermolecular salt bridge with the side chain of Glu136 and another hydrogen bond with the side chain of $_L$Glu58. It is, however, poorly justified to speculate on the significance of the observed adjustment within the $_L$Arg113 side chain in complex formation, since the orientation of this

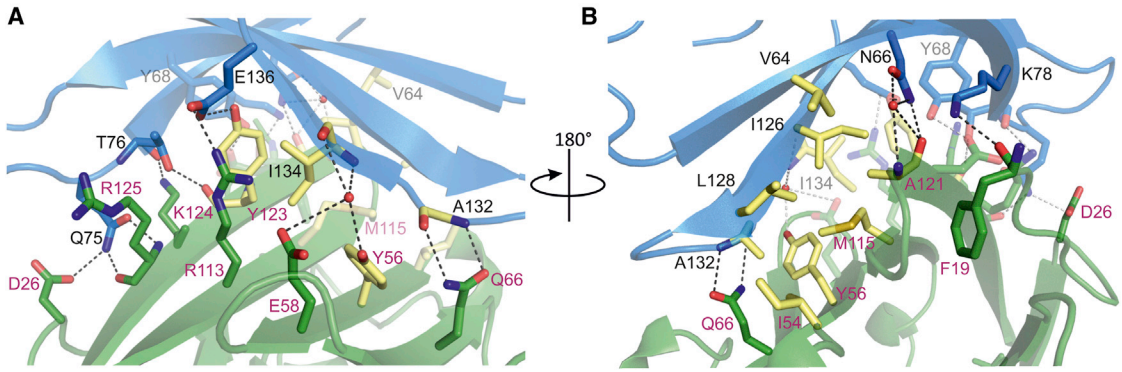

Figure 2. Close-Up Views of the hPD-1/hPD-L1 Interface

hPD-1 and hPD-L1 are represented by blue and green ribbons, respectively. All residues important for the interaction are highlighted as sticks. Residues forming the hydrophobic core are colored yellow. Water molecules are shown as red spheres. Hydrogen bonds are depicted as black dashed lines.

(A) Front-side view.

(B) Back-side view.

residue is likely affected by crystal packaging in the structure of apo-hPD-L1. Moreover, $_{L}$Arg113 assumes a yet different conformation within the mPD-1/hPD-L1 structure.

Detailed Analysis of the Receptor-Ligand Interactions

The crystal structure determined in this study demonstrates that the receptor-ligand interaction is mediated in its major part by residues of C′CFG strands within both PD-1 and PD-L1 (Figure 2). The protein-protein contacts involve both hydrophobic interactions and polar interactions, and bury a total surface area of 1,970 Å^2. The interaction is constructed around a central hydrophobic core contributed by both partners and constituted by nonpolar residues in the front sheet of PD-1 (Val64, Ile126, Leu128, Ala132, Ile134) and those of the front sheet of PD-L1 ($_{L}$Ile54, $_{L}$Tyr56, $_{L}$Met115, $_{L}$Ala121, $_{L}$Tyr123), including a characteristic alkyl-π interaction of the side chains of Ile134 and $_{L}$Tyr123. This hydrophobic region is open to the solvent on the would-be antigen-binding site, and is neighbored by a buried region of mixed polar/nonpolar interactions on the opposite side of the molecule. Both these regions are surrounded by a peripheral network of polar residues (safe on the CDR loop side) providing additional hydrogen bond-mediated interactions between the receptor and the ligand.

The region of mixed polar/nonpolar contacts buried deep within the binding interface consists of a pronounced π-π stacking interaction between the side chains of Tyr68 and $_{L}$Tyr123 where the two phenol groups are oriented antiparallel, thereby optimizing dipole momentum (Figure S3). In addition, the hydroxyl within the side chain of Tyr68 makes a hydrogen bond contact with the side-chain carboxyl of $_{L}$Asp122, and a comparable contact is observed between the side-chain hydroxyl of $_{L}$Tyr123 and the side-chain carboxyl of Glu136, which makes this entire interaction region roughly pseudo-symmetrical. Furthermore, a buried hydrogen bond between the side chain of Asn66 and the carbonyl main-chain oxygen of $_{L}$Ala121 additionally contributes to the hPD-1/hPD-L1 interaction.

The polar interactions located at the periphery of the interface and, therefore, partially exposed to the solvent, include a hydrogen bond between the backbone amide of Ala132 and side-chain carbonyl atom of $_{L}$Gln66, water-mediated interactions between the backbone amide and carbonyl of Ile134 and $_{L}$Tyr56 hydroxyl and $_{L}$Glu58 carboxyl, and a salt bridge maintained between Glu136 and $_{L}$Arg113 at the front side of the complex (Figure 2A). Hydrogen bonds connecting the side chain of Thr76 and backbone carbonyl oxygen of $_{L}$Tyr123, the side chain of Gln75 and backbone amide and carbonyl of $_{L}$Arg125, and an additional hydrogen bond between the side chains of Gln75 and $_{L}$Asp26 form the interactions at the side of the complex opposite to the CDR loops. Furthermore, hydrogen bonds between the backbone carbonyl oxygen of Thr76 and the side-chain amine of $_{L}$Lys124, the side-chain amine of Lys78 and backbone carbonyl oxygen of $_{L}$Phe19, and a water-mediated interaction of the side chain of Asn66 and the main-chain carbonyl oxygen of $_{L}$Ala121 stabilize the interaction on the back side of the complex (Figure 2B).

DISCUSSION

Given the spectacular results obtained in clinics by the antibodies that target the PD-1/PD-L1 axis and the fact that small-molecule inhibitors of protein-protein interactions proved promising drug candidates, it is not surprising that groups in academia, pharmaceutics, and biotech companies have ongoing projects on the PD-1 small-molecule inhibitors. None of these groups, however, including ours, have reported such inhibitors until now. One of the reasons for this may have been that the structural information derived from the complex with murine PD-1 suggested a pharmacophore for the design of leads for PD-1 that, in light of our structure of the human complex, may not have been suitable for finding small molecules that bind to the human protein.

The protein-protein interaction surface is notoriously difficult to target with small molecules, and usually the structures of individual components are not sufficient to guide rational inhibitor design. This is because the hydrophobic interaction surface found within the complex is often involved in crystal contacts in the apo forms, which may result in certain

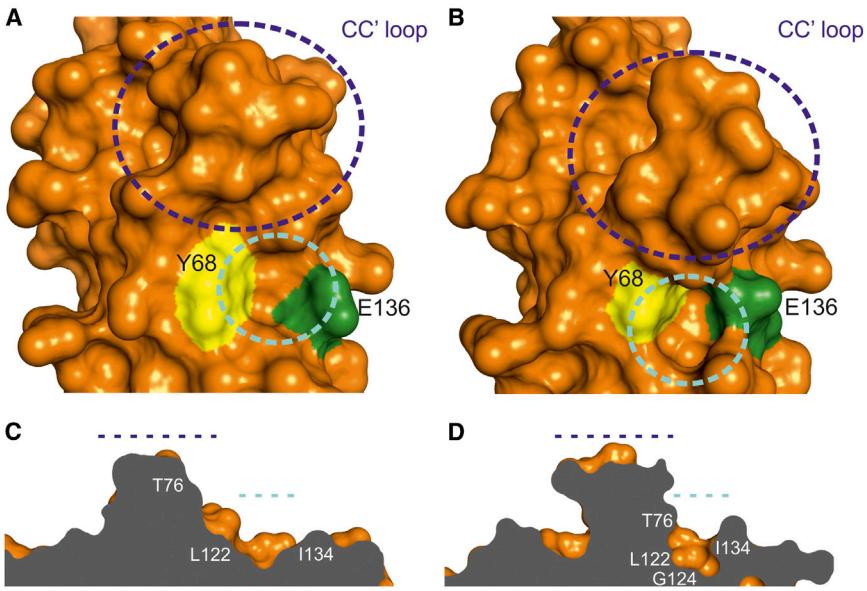

Figure 3. Gly124 Cleft (LTyr123-Accommodating Cavity) and CC′ Loop Rearrangement Are Induced by hPD-L1 Binding to hPD-1

(A and B) Surface representation of the hPD-L1 binding site of hPD-1. (A) Apo-hPD-1. (B) hPD-1 complexed with hPD-L1. The CC′ loop is marked by the blue circle, the LTyr123-accommodating cavity (i.e. the Gly124 cleft) is marked by a cyan circle; Tyr68 and Glu136 are marked in yellow and green, respectively.

(C and D) Cross sections through CC′ loop (blue line) and Gly124 cleft (cyan line) of hPD-1 structures shown in (A) and (B), respectively, depicting rearrangement of the interaction surface upon ligand binding.

artifactual conclusions. Moreover, significant plasticity within the components usually accompanies the complex formation. Therefore, complete information is provided only by comparing experimentally determined structures of components in their apo forms (preferably in multiple crystal forms) and their complex. To this end, the structure of mPD-1/hPD-L1 complex has been determined previously. However, relatively low sequence identity of mouse and human PD-1 suggested likely differences in the detailed binding modes. Consistently, the structures of apo-hPD-1 and that of its murine ortholog are dissimilar in that the human receptor lacks a C″ strand within its Ig V-type fold (which is replaced by a flexible loop connecting the C′ and D strands), the BC loops adopt different conformations, and some important residues forming the interaction surface are different within the orthologs. Therefore, although mutagenesis studies and nuclear magnetic resonance (NMR) data have suggested that the overall binding mode of hPD-1 and hPD-L1 is consistent with that of mouse-derived receptor and a human-derived ligand, the detailed molecular features of the former interaction have remained unknown prior to this study.

Here, we show that structural differences between human and murine apo-PD-1 correspond to certain differences within the detailed binding modes to hPD-L1. First, the interaction surface within the human complex is notably different from that published previously for the m/h complex (Figure S3). Second, plasticity in the PD-1 receptor is seen in the complex formation within human protein, which is not the case for the m/h complex. Comparison of the interaction surface between apo and complexed hPD-1 (Figure 3) shows changes associated with remodeling upon binding of the ligand. The surface segment formed by Tyr68, Ile134, and Glu136 in the apoprotein undergoes rearrangement upon ligand binding. LTyr123 forces the deepening of the cleft by jostling Leu122, Cys123, and Gly124 residues of the F strand, thereby changing the position of the side chain of Ile134 (and Glu136) and enforcing closure of the CC′ loop (Figures 1 and 3). These data allow for determining the hPD1/hPD-L1 protein-protein interaction hot spots (Guo et al., 2014; Koes et al., 2012).

The hPD-1 hot spots are mostly hydrophobic and comprise Asn66, Tyr68, Gly124, Ile126, Leu128, Ile134, and Glu136 located in the front sheet of hPD-1. The most distinctive feature of this segment is the hydrophobic cleft at Gly124. The interface here relies on the steric complementarity between the PD-1 cleft and the hydrophobic face of the hPD-L1 and, in particular, on LTyr123, which inserts deep in the Gly124 cleft. With the aromatic ring of Tyr68 on one side and the backbone of Glu136 on the other side of the groove, the cleft is a perfect spot for anchoring an aromatic ring. Pointing toward Asn66, Ile126, and Leu128 in one direction and toward Met70-Asp77 to close the CC′ loop in another, such a chemical probe may easily cover almost all important interactions within the Gly124 anchor site.

The fragment-based lead design has become an important and powerful approach in structure-based lead discovery (reviewed in Hajduk and Greer, 2007; Murray et al., 2012). Starting fragments have low molecular mass (<300 Da), and although the binding interactions of these fragments with target proteins are weak (in the millimolar range), they are structurally understood through X-ray crystallography or NMR and exhibit high ‘‘ligand efficiency’’. For example, tyrosine derivatives that mimic the anchor residue LTyr123 that fills the Gly124 pocket in the PD-1/PD-L1 complex should in principle be an excellent building block of such fragments. We have tested a limited number of tyrosine derivatives for their anticipated interaction with hPD-1, but without success (Table S1). In the structure of the apo-PD-1, the pocket we attempted to target is only partly formed owing to the intrinsic flexibility of the CC′ loop. Since the ‘‘open conformation’’ of the CC′ loop in PDB: 3RRQ is partly stabilized by crystal packing, it may not be excluded that there is an ensemble of open and closed conformations of the CC′ loop of human PD-1 in solution. Targeting the transient states of this pocket with fragments may therefore be challenging. Fragment ligands with weak affinities might not provide sufficient binding free energy to sustain permanent loop closure that hPD-1 exhibits when binding to hPD-L1, which generates a favorable binding pocket on an otherwise relatively flat surface. A larger number of analogs needs to be tested, however, to confirm such a

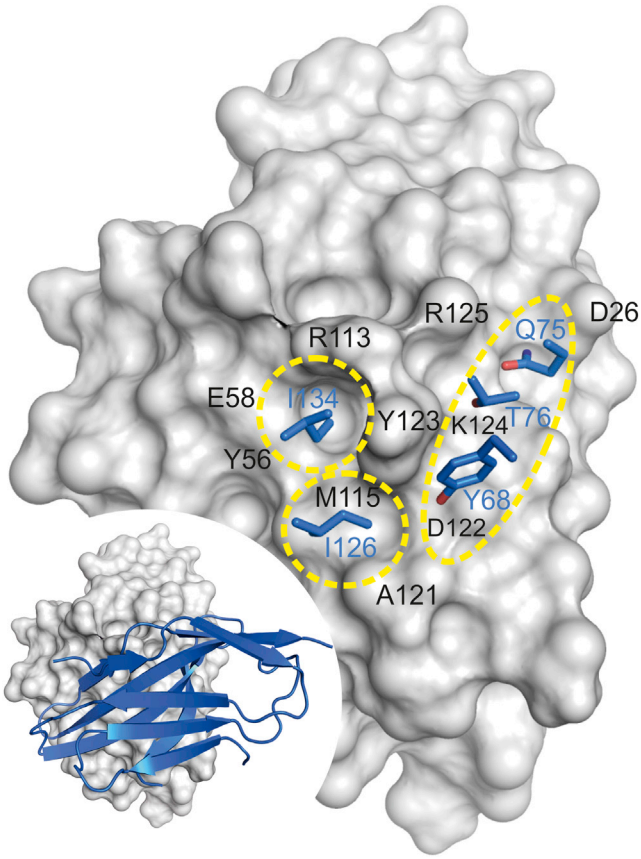

Figure 4. Three Main Hot Spots on the PD-L1 Surface

The deepest cleft comprises $_L$Tyr56, $_L$Glu58, $_L$Arg113, $_L$Tyr123, and $_L$Met115. The second hot spot is formed by $_L$Met115, $_L$Ala121, and $_L$Tyr123. The third hot spot, constituted by a shallow groove, is composed of $_L$Asp122-$_L$Arg125 and $_L$Asp26. Residues from hPD-1 are colored blue, hPD-L1 is represented by gray surface, and the hot spots are marked by yellow circles. General orientation of the PD-1/PD-L1 complex is represented in the bottom left corner.

hypothesis. Also, larger small molecules may possibly more easily mimic the effect of the binding of PD-L1 to PD-1 (i.e., the fragments that additionally interact with the residues of the CC′ loop).

Within the hPD-1 interaction surface of hPD-L1 we identified three major hot spots, two of which are expected to form a druggable pharmacophore (Figure 4). The first is a classical pocket of mostly hydrophobic character accommodating Ile134. This pocket is composed of the side chains of $_L$Tyr56, $_L$Glu58, $_L$Arg113, $_L$Met115, and $_L$Tyr123, and is of perfect size and properties to accommodate a six-membered aromatic ring (we designate this pocket the Ile134 pocket). The second hot spot is located just nearby and accommodates Ile126. It is composed of $_L$Met115, $_L$Ala121, and $_L$Tyr123, and could likely be effectively filled by a branched aliphatic moiety, which could anchor with a terminal hydrogen bond donor group at carbonyl oxygen of $_L$Ala121. The third hot spot is an extended groove accommodating Tyr68, Gln75, and Thr76. It is formed by the main chain and the side chains spanning residues $_L$Asp122 to $_L$Arg125, and is flanked by the side chain of $_L$Asp26. Multiple hydrogen bond donors and acceptors are available within the groove, which is, however, relatively shallow and may be hard to efficiently target with small-molecule probes.

In summary, the data presented here provide the structural basis for the rational design of small-molecule therapeutics that disrupt the PD-1/PD-L1 interaction.

EXPERIMENTAL PROCEDURES

Protein Expression and Purification

The interacting extracellular domains of hPD-1 (residues 33–150; UniProt: Q15116; cysteine at position 93 was replaced with serine to aid protein stability) and hPD-L1 (residues 18–134; UniProt: Q9NZQ7) were cloned into pET-24d and pET-21b, respectively and expressed in *Escherichia coli* BL21 (DE3) in the form of inclusion bodies (IB). IB were collected, washed, and dissolved in buffered guanidine hydrochloride. Both proteins were refolded by dropwise dilution followed by dialysis, and purified to homogeneity by gel filtration. The purity and protein folding were evaluated by SDS-PAGE and NMR, respectively.

Crystallization of the hPD-1/hPD-L1 Complex and Apo-hPD-L1

Purified hPD-1 and hPD-L1 were mixed in 1:1 molar ratio, and the complex was purified by gel filtration in 10 mM Tris (pH 8.0) containing 20 mM NaCl. Complex-containing fractions were pooled and concentrated to 3 mg/ml. Diffraction-quality crystals were obtained at room temperature from 0.1 M Bis-Tris (pH 5.5) containing 1.84 M ammonium sulfate using a sitting-drop vapor diffusion setup. Apo-hPD-L1 was concentrated to 5 mg/ml, and diffraction-quality crystals were obtained from 1.80 M sodium formate using similar methodology.

Structure Determination and Refinement

Crystals were flash-cooled in liquid nitrogen after cryoprotection. The diffraction data were collected at the Helmholtz Centrum 14.1 beamline at BESSY (Berlin, Germany; Mueller et al., 2015). The data were indexed and integrated using XDS (Krug et al., 2012; Kabsch, 2010), and scaled and merged using Scala (Evans, 2006). The initial phases were obtained by molecular replacement calculated using Phaser (McCoy et al., 2007). The models were manually built in the resulting electron density maps using Coot (Emsley et al., 2010). Restrained refinement was performed using Phenix (Adams et al., 2010) and Refmac 5.0 (Murshudov et al., 2011). The final models were deposited in the PDB under accession numbers PDB: 4ZQK and 5C3T.

Details of the expression and purification of hPD-1 and hPDL-1, crystallization of the hPD-1/hPD-L1 complex and apo-hPD-L1, and structure solution and refinement are described in Supplemental Experimental Procedures. Data collection and refinement statistics are summarized in Table 1.

ACCESSION NUMBERS

Coordinates and structure factors have been deposited in the PDB under accession codes PDB: 4ZQK and 5C3T.

SUPPLEMENTAL INFORMATION

Supplemental Information includes Supplemental Experimental Procedures, four figures, and one table and can be found with this article online at http://dx.doi.org/10.1016/j.str.2015.09.010.

ACKNOWLEDGMENTS

This research has been supported (to T.A.H.) by a Marie Curie FP7-Reintegration-Grant within the seventh European Community Framework Program, by the UMO-2012/06/A/ST5/00224 grant from the National Science Center, and by the Project operated within the Foundation for Polish Science TEAM Program, co-financed by the EU European Regional Development Fund; and (to A.D.) by the NIH grants 1R21GM087617, 1R01GM097082, and 1P41GM094055; and (to G.D.) UMO-2011/01/D/NZ1/01169 from the National Science Center and (to K.M.Z.) grant BMN 6/2014 for the Development of Young Scientists from FBBB UJ. P.G. was supported by the European Union

within the SET project. The X-ray data were collected at the BESSY II 14.1 beamline at Helmholtz-Zentrum Berlin für Materialien und Energie (HZB).

Received: July 17, 2015
Revised: August 27, 2015
Accepted: September 3, 2015
Published: October 22, 2015

REFERENCES

Adams, P.D., Afonine, P.V., Bunkóczi, G., Chen, V.B., Davis, I.W., Echols, N., Headd, J.J., Hung, L.W., Kapral, G.J., Grosse-Kunstleve, R.W., et al. (2010). PHENIX: a comprehensive Python-based system for macromolecular structure solution. Acta Crystallogr. D Biol. Crystallogr. *66*, 213–221.

Ahmadzadeh, M., Johnson, L.A., Heemskerk, B., Wunderlich, J.R., Dudley, M.E., White, D.E., and Rosenberg, S.A. (2009). Tumor antigen-specific CD8 T cells infiltrating the tumor express high levels of PD-1 and are functionally impaired. Blood *114*, 1537–1544.

Barber, D.L., Wherry, E.J., Masopust, D., Zhu, B., Allison, J.P., Sharpe, A.H., Freeman, G.J., and Ahmed, R. (2006). Restoring function in exhausted CD8 T cells during chronic viral infection. Nature *439*, 682–687.

Brahmer, J.R., Tykodi, S.S., Chow, L.Q., Hwu, W.J., Topalian, S.L., Hwu, P., Drake, C.G., Camacho, L.H., Kauh, J., Odunsi, K., et al. (2012). Safety and activity of anti-PD-L1 antibody in patients with advanced cancer. N. Engl. J. Med. *366*, 2455–2465.

Chen, D.S., and Mellman, I. (2013). Oncology meets immunology: the cancer-immunity cycle. Immunity *39*, 1–10.

Chen, Y., Liu, P., Gao, F., Cheng, H., Qi, J., and Gao, G.F. (2010). A dimeric structure of PD-L1: functional units or evolutionary relics? Protein Cell *1*, 153–160.

Cheng, X., Veverka, V., Radhakrishnan, A., Waters, L.C., Muskett, F.W., Morgan, S.H., Huo, J., Yu, C., Evans, E.J., Leslie, A.J., et al. (2013). Structure and interactions of the human programmed cell death 1 receptor. J. Biol. Chem. *288*, 11771–11785.

Dömling, A., and Holak, T.A. (2014). Programmed death-1: therapeutic success after more than 100 years of cancer immunotherapy. Angew. Chem. Int. Ed. Engl. *53*, 2286–2288.

Emsley, P., Lohkamp, B., Scott, W.G., and Cowtan, K. (2010). Features and development of Coot. Acta Crystallogr. D Biol. Crystallogr. *66*, 486–501.

Evans, P.R. (2006). Scaling and assessment of data quality. Acta Crystallogr. D Biol. Crystallogr. *62*, 72–82.

Freeman, G.J. (2008). Structures of PD-1 with its ligands: sideways and dancing cheek to cheek. Proc. Natl. Acad. Sci. USA *105*, 10275–10276.

Guo, W.X., Wisniewski, J.A., and Ji, H. (2014). Hot spot-based design of small-molecule inhibitors for protein-protein interactions. Bioorg. Med. Chem. Lett. *24*, 2546–2554.

Hajduk, P.J., and Greer, J. (2007). A decade of fragment-based drug design: strategic advances and lessons learned. Nat. Rev. Drug Discov. *6*, 211–219.

Hamid, O., Robert, C., Daud, A., Hodi, F.S., Hwu, W.J., Kefford, R., Wolchok, J.D., Hersey, P., Joseph, R.W., Weber, J.S., et al. (2013). Safety and tumor responses with lambrolizumab (anti-PD-1) in melanoma. N. Engl. J. Med. *369*, 134–144.

Hawkes, E.A., Grigg, A., and Chong, G. (2015). Programmed cell death-1 inhibition in lymphoma. Lancet Oncol. *16*, 234–235.

Herbst, R.S., Soria, J.C., Kowanetz, M., Fine, G.D., Hamid, O., Gordon, M.S., Sosman, J.A., McDermott, D.F., Powderly, J.D., Gettinger, S.N., et al. (2014). Predictive correlates of response to the anti-PD-L1 antibody MPDL3280A in cancer patients. Nature *515*, 563–567.

Inman, B.A. (2007). PD-L1 (B7-H1) expression by urothelial carcinoma of the bladder and BCG-induced granulomata: associations with localized stage progression. Cancer *109*, 1499–1505.

Kabsch, W. (2010). XDS. Acta Crystallogr. D Biol. Crystallogr. *66*, 125–132.

Koes, D., Khoury, K., Huang, Y., Wang, W., Bista, M., Popowicz, G.M., Wolf, S., Holak, T.A., Dömling, A., and Camacho, C.J. (2012). Enabling large-scale design, synthesis and validation of small molecule protein-protein antagonists. PLoS One *7*, e32839.

Krug, M., Weiss, M.S., Heinemann, U., and Mueller, U. (2012). XDSAPP: a graphical user interface for the convenient processing of diffraction data using XDS. J. Appl. Crystallogr. *45*, 568–572.

Lázár-Molnár, E., Yan, Q., Cao, E., Ramagopal, U., Nathenson, S.G., and Almo, S.C. (2008). Crystal structure of the complex between programmed death-1 (PD-1) and its ligand PD-L2. Proc. Natl. Acad. Sci. USA *105*, 10483–10488.

Lin, D.Y., Tanaka, Y., Iwasaki, M., Gittis, A.G., Su, H.P., Mikami, B., Okazaki, T., Honjo, T., Minato, N., and Garboczi, D.N. (2008). The PD-1/PD-L1 complex resembles the antigen-binding Fv domains of antibodies and T cell receptors. Proc. Natl. Acad. Sci. USA *105*, 3011–3016.

Lipson, E.J., and Drake, C.G. (2011). Ipilimumab: an anti-CTLA-4 antibody for metastatic melanoma. Clin. Cancer Res. *17*, 6958–6962.

Mahoney, K.M., Freeman, G.J., and McDermott, D.F. (2015). The Next immune-checkpoint inhibitors: PD-1/PD-L1 blockade in melanoma. Clin. Ther. *37*, 764–782.

Matsuzaki, J., Gnjatic, S., Mhawech-Fauceglia, P., Beck, A., Miller, A., Tsuji, T., Eppolito, C., Qian, F., Lele, S., Shrikant, P., et al. (2010). Tumor-infiltrating NY-ESO-1-specific CD8+ T cells are negatively regulated by LAG-3 and PD-1 in human ovarian cancer. Proc. Natl. Acad. Sci. USA *107*, 7875–7880.

McCoy, A.J., Grosse-Kunstleve, R.W., Adams, P.D., Winn, M.D., Storoni, L.C., and Read, R.J. (2007). Phaser crystallographic software. J. Appl. Crystallogr. *40*, 658–674.

Moreno, B.H., and Ribas, A. (2015). Anti-programmed cell death protein-1/ligand-1 therapy in different cancers. Br. J. Cancer *112*, 1421–1427.

Mueller, U., Förster, R., Hellmig, M., Huschmann, F.U., Kastner, A., Malecki, P., Pühringer, S., Röwer, M., Sparta, K., Steffien, M., et al. (2015). The macromolecular crystallography beamlines at BESSY II of the Helmholtz-Zentrum Berlin: current status and perspectives. Eur. Phys. J. Plus *130*, 141.

Muenst, S., Soysal, S.D., Gao, F., Obermann, E.C., Oertli, D., and Gillanders, W.E. (2013). The presence of programmed death 1 (PD-1)-positive tumor-infiltrating lymphocytes is associated with poor prognosis in human breast cancer. Breast Cancer Res. Treat. *139*, 667–676.

Murray, C.W., Verdonk, M.L., and Rees, D.C. (2012). Experiences in fragment-based drug discovery. Trends Pharmacol. Sci. *33*, 224–232.

Murshudov, G.N., Skubák, P., Lebedev, A.A., Pannu, N.S., Steiner, R.A., Nicholls, R.A., Winn, M.D., Long, F., and Vagin, A.A. (2011). REFMAC5 for the refinement of macromolecular crystal structures. Acta Crystallogr. D Biol. Crystallogr. *67*, 355–367.

Phan, T.G., Long, G.V., and Scolyer, R.A. (2015). Multiple checkpoints on the long road towards cancer immunotherapy. Immunol. Cell Biol. *93*, 323–325.

Powles, T., Eder, J.P., Fine, G.D., Braiteh, F.S., Loriot, Y., Cruz, C., Bellmunt, J., Burris, H.A., Petrylak, D.P., Teng, S.L., et al. (2014). MPDL3280A (anti-PD-L1) treatment leads to clinical activity in metastatic bladder cancer. Nature *515*, 558–562.

Riella, L.V., Paterson, A.M., Sharpe, A.H., and Chandraker, A. (2012). Role of the PD-1 pathway in the immune response. Am. J. Transplant. *12*, 2575–2587.

Sakuishi, K., Apetoh, L., Sullivan, J.M., Blazar, B.R., Kuchroo, V.K., and Anderson, A.C. (2010). Targeting Tim-3 and PD-1 pathways to reverse T cell exhaustion and restore anti-tumor immunity. J. Exp. Med. *207*, 2187–2194.

Schumacher, T.N., Kesmir, C., and van Buuren, M.M. (2015). Biomarkers in cancer immunotherapy. Cancer Cell *27*, 12–14.

Schwartz, J.C., Zhang, X., Fedorov, A.A., Nathenson, S.G., and Almo, S.C. (2001). Structural basis for co-stimulation by the human CTLA-4/B7-2 complex. Nature *410*, 604–608.

Stamper, C.C., Zhang, Y., Tobin, J.F., Erbe, D.V., Ikemizu, S., Davis, S.J., Stahl, M.L., Seehra, J., Somers, W.S., and Mosyak, L. (2001). Crystal structure of the B7-1/CTLA-4 complex that inhibits human immune responses. Nature *410*, 608–611.

Sun, S., Fei, X., Mao, Y., Wang, X., Garfield, D.H., Huang, O., Wang, J., Yuan, F., Sun, L., Yu, Q., et al. (2014). PD-1+ immune cell infiltration inversely

correlates with survival of operable breast cancer patients. Cancer Immunol. Immunother. *63*, 395–406.

Topalian, S.L., Drake, C.G., and Pardoll, D.M. (2015). Immune checkpoint blockade: a common denominator approach to cancer therapy. Cancer Cell *27*, 450–461.

Tumeh, P.C., Harview, C.L., Yearley, J.H., Shintaku, I.P., Taylor, E.J., Robert, L., Chmielowski, B., Spasic, M., Henry, G., Ciobanu, V., et al. (2014). PD-1 blockade induces responses by inhibiting adaptive immune resistance. Nature *515*, 568–571.

Wherry, E.J. (2011). T cell exhaustion. Nat. Immunol. *12*, 492–499.

Zhang, X., Schwartz, J.C., Guo, X., Bhatia, S., Cao, E., Lorenz, M., Cammer, M., Chen, L., Zhang, Z.Y., Edidin, M.A., et al. (2004). Structural and functional analysis of the costimulatory receptor programmed death-1. Immunity *20*, 337–347.

